Journal of Sound and Vibration 329 (2010) 980–993

Contents lists available at ScienceDirect

Journal of Sound and Vibration

journal homepage: www.elsevier.com/locate/jsvi

Minimisation of the sound power radiated by a submarine through optimisation of its resonance changer

Sascha Merz [a,*], Nicole Kessissoglou [a], Roger Kinns [a], Steffen Marburg [b]

[a] School of Mechanical and Manufacturing Engineering, University of New South Wales, Sydney, NSW 2052, Australia
[b] Insititut für Festkörpermechanik, Technische Universität, Mommsenstr. 13, 01062 Dresden, Germany

ARTICLE INFO

Article history:
Received 31 May 2009
Received in revised form
12 October 2009
Accepted 13 October 2009
Handling Editor: L.G. Tham
Available online 2 November 2009

ABSTRACT

An important cause of sound radiation from a submarine in the low frequency range is fluctuating forces at the propeller. The forces are transmitted to the hull via the shaft and the fluid. Sound radiation occurs due to hull and propeller vibrations as well as dipole sound radiation caused by the operation of the propeller in a non-uniform wake. In order to minimise sound radiation caused by propeller forces, a hydraulic vibration attenuation device known as a resonance changer can be implemented in the propeller/shafting system. In this work, cost functions that represent the overall radiated sound power are investigated, where the virtual stiffness, damping and mass of the resonance changer were chosen as design parameters. The minima of the cost functions are found by applying gradient based optimisation techniques. The finite element and boundary element methods are used to model the structure and the fluid, respectively. The adjoint operator is employed to calculate the sensitivity of the cost function to the design parameters. The influence of sound radiation due to propeller vibration on the optimisation of the resonance changer as well as the influence of the reduction in amplitude for higher harmonics of the blade-passing frequency on the control performance is investigated.

© 2009 Elsevier Ltd. All rights reserved.

1. Introduction

As a submarine is subject to detection by passive sonar, reduction of the overall radiated sound power is desired. A significant proportion of the radiated sound power is caused by operation of the propeller in a spatial non-uniform wake [1,2]. As the propeller blades pass through sections of different volume flow rate, they experience a temporal variation in drag. This results in a harmonically varying force on the propeller shaft as well as a harmonically varying pressure field originating from the propeller, at the blade-passing frequency (*bpf*) and its multiples. The propeller pressure field as well as the structural force can excite hull accordion modes, which are efficient sound radiators [3]. Furthermore, the structural force causes axial vibration of the propeller/propulsion system, leading to additional sound radiation from the propeller and hence re-excitation of the pressure hull. The sound power radiated by the submarine is due to the combination of the sound fields radiated by the propeller and the hull.

In order to reduce the radiated sound power, a vibro-acoustic model of the submarine and sea water has been developed to minimise a cost function that represents the radiated sound power over a given frequency range [4]. For cruise speeds where no cavitation at the propeller tips occurs, the frequency range up to 100 Hz is of interest, where the first four harmonics of *bpf* are taken into account. The complete frequency spectrum needs to be considered for optimisation

* Corresponding author.
E-mail address: sascha.merz@gmx.net (S. Merz).

0022-460X/$ - see front matter © 2009 Elsevier Ltd. All rights reserved.
doi:10.1016/j.jsv.2009.10.019

procedures, as the *bpf* varies with cruise speed. The fluctuating forces at the propeller are assumed to be harmonic and linear. Hence, the analysis has been conducted in the frequency domain using the Helmholtz equation for the exterior radiation/scattering problem. The submarine is a complex, non-homogeneous structure, but its different parts may be represented by simplified physical models such as shells, rods and spring–mass–damper systems. The numerical approach used here to solve the strong fully coupled structure/fluid problem in the low frequency range, where the densities of the structure and the fluid are of similar order, is the combination of the finite element (FE) method to represent the structure and the boundary element (BE) method to represent the fluid [5–7].

The propeller/shafting system comprises the propeller, propeller shaft, thrust bearing, foundation and a device known as a resonance changer (RC), which acts as a dynamic hydraulic vibration absorber. Goodwin suggested to tune the RC such that its natural frequency equals that of the propeller/shafting system [8]. Dylejko developed simplified, analytical submarine models to find optimum design parameters for different RC configurations in order to minimise the maximum radiated sound pressure rather than the overall radiated sound power [9,10]. A genetic optimisation strategy was used for the optimisation process. Due to simplifications in the analytical models such as omission of the tailcone and pressure field from the propeller, the complex interaction between the propeller and the submarine hull was not taken into account.

In contrast to analytical methods, numerical methods allow for the development of more detailed and complex structural models. However, the computational cost is much higher and non-gradient based optimisation methods such as genetic algorithms used in Ref. [10] are not viable. Hence, gradient based optimisation techniques are preferred and the sensitivity of the cost function to structural design parameters is computed. In previous work by the authors, the structural and acoustic responses of a submarine were presented for fixed parameters of the RC, where excitation of the submarine hull due to fluid forces was taken into account [11]. In this paper, the focus is on optimising the RC parameters of a submarine model, where the significance of hull excitation due to propeller forces via the fluid is of particular interest. Numerical models of the sound power radiated by a submarine are presented, where the sensitivity of the weighted sound power over the relevant frequency range to design parameters of the propeller/shafting system has been computed. The sensitivity is obtained in a semi-analytical way by employing the adjoint operator [4]. Optimum parameters are found for the virtual stiffness, damping and mass of the RC by applying the globally convergent method of moving asymptotes [12].

2. Simplified physical model of the submarine

A simplified physical model of a submarine has been developed previously by the authors as shown in Fig. 1 [11]. The pressure hull was modelled as a thin-walled cylinder with evenly spaced ring-stiffeners of rectangular cross-section and two evenly spaced circular plates that represent the bulkheads. As the end plates of a submarine pressure hull are stiff in comparison to other parts, they have been modelled as rigid plates. In order to account for the contribution of the on-board machinery and internal structure to the dynamic behaviour of the submarine, a distributed mass has been attached to the cylindrical shell of the pressure hull.

The propeller/shafting system was modelled in a modular manner as shown in Fig. 2 [9], where the propeller force and velocity amplitude are given by f_p and v_p, respectively. The hull drive point force and velocity are denoted by f_h and v_h. The propeller as well as the added mass effect of the surrounding water for the propeller are represented by a lumped mass m_p. The propeller dimensions for calculating the propeller mass and the fluid loading effect are chosen by assuming that the propeller volume is $\frac{1}{1000}$ of the volume displaced by the pressure hull. The propeller diameter is assumed to be half the pressure hull diameter. The propeller shaft was modelled as a simple rod with an effective length l_{se} and an overall length l_s as shown in Fig. 2, where the overhang was represented by a lumped mass. The shaft properties are also defined by its cross-sectional area A_s, Young's modulus E_s and density ρ_s. The thrust bearing was assumed to act as a spring–mass–damper system with mass m_b, damping coefficient c_b and spring constant k_b. For the present model, the thrust bearing is attached to a single resonance changer that has been modelled as a spring–mass–damper system according to Goodwin [8]. The RC is represented by virtual mass, damper and spring parameters, which are calculated by [8]

$$m_r = \frac{\rho_r A_0^2 L}{A_1}, \quad c_r = 8\pi\mu L \frac{A_0^2}{A_1^2}, \quad k_r = \frac{A_0^2 B}{V}. \tag{1}$$

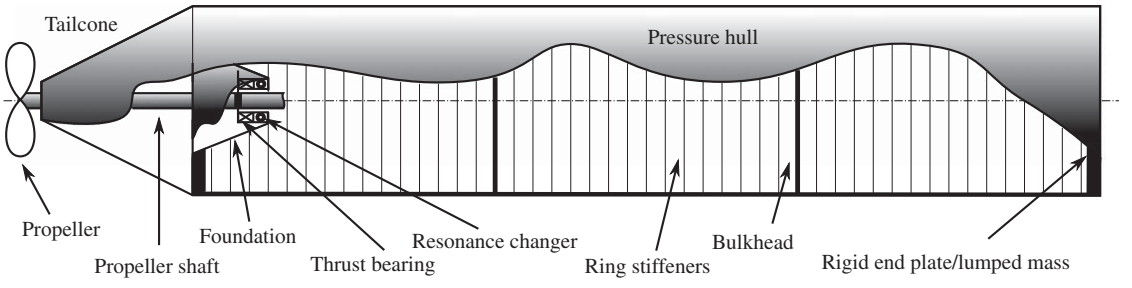

Fig. 1. Simplified physical model of the submarine.

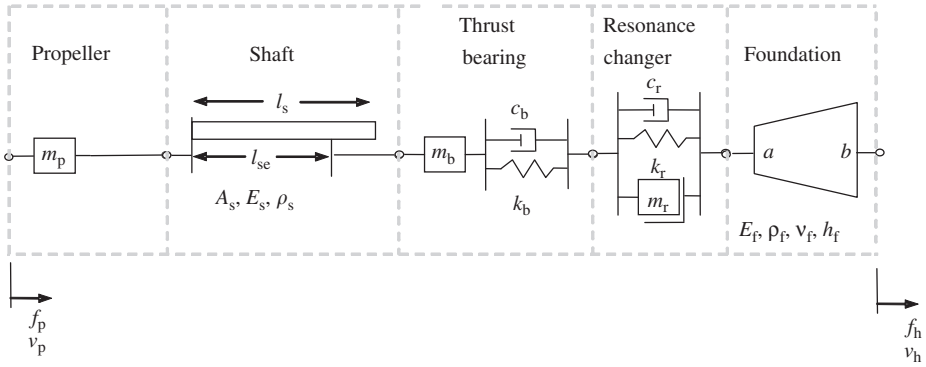

Fig. 2. Modular approach for the propeller/shafting system [9].

ρ_r is the density of the hydraulic medium, μ is the dynamic viscosity and B is the bulk modulus of the oil in the RC. V is the volume of the reservoir, A_1 is the cross-sectional area of the pipe, L is the pipe length and A_0 is the cross-sectional area of the cylinder.

The foundation is simplified as a truncated cone for the axisymmetric model with end radii a and b as shown in Fig. 2. Young's modulus, density, Poisson's ratio and thickness of the foundation are given by E_f, ρ_f, ν_f and h_f, respectively.

An analytical model for the sound field radiated by the propeller is presented in Ref. [11]. The sound field is the combination of contributions from (i) the hydrodynamic mechanism that arises from the propeller operating in a non-uniform wake and (ii) the axial fluctuation of the propeller due to vibration of the propeller/shafting system. The sound radiation that corresponds to the axial force on the propeller hub is given by the dipole

$$p(r,\theta) = \mathrm{j}kg(r)f\left(1-\frac{\mathrm{j}}{kr}\right)\mathrm{D}(\theta), \tag{2}$$

where k is the fluid wavenumber, θ is the angle between the field point direction and the force direction, f is the amplitude of the exciting force, r is the distance between the source and the field point, $\mathrm{D}(\theta)=\cos\theta$ is the directivity function and

$$g(r) = \frac{\mathrm{e}^{-\mathrm{j}kr}}{4\pi r} \tag{3}$$

is the free space Green's function.

The contribution due to (ii) resulting from vibration of the propeller can be computed using a rigid disc approximation. The pressure is also given by Eq. (2) and the directivity function is [13]

$$\mathrm{D}(\theta) = \frac{2\mathrm{J}_1(ka\sin\theta)}{ka\cos\theta} \approx \cos\theta, \text{ small } ka, \tag{4}$$

where J_1 is the first-order Bessel-function and a is the disc radius. The force acting on the fluid is obtained in terms of the axial propeller velocity v_p by

$$f = 2sz_cz_av_p, \tag{5}$$

where $s=\pi a^2$ is the area of the disc surface, z_c is the characteristic impedance of the fluid and z_a is the radiation impedance. The radiation impedance can be expressed as the sum of its real and imaginary parts, corresponding to the resistance r_a and the reactance x_a, respectively. The resistance and reactance can be obtained under the assumption that a freely suspended disc has twice the admittance of a disc in an infinite baffle [14]. For small ka, this gives

$$r_a = \frac{8(ka)^4}{27\pi^2}, \quad x_a = \frac{4ka}{3\pi}. \tag{6}$$

3. Numerical modelling

3.1. Combined FE/BE model

In this work, the radiated sound power from a coupled vibro-acoustic system with additional discrete sources in the fluid domain has been evaluated. This was accomplished by representation of the structure using finite elements and representation of the fluid using boundary elements, where strong coupling is considered at the structure/fluid interface [11]. Strong coupling involves the acoustic medium influencing the dynamic behaviour of the structure, as the densities of

fluid and structure are of similar order. Under the assumption that an acoustically hard surface is present, the continuity condition requires that the displacement of the fluid equals the displacement of the structure normal to the surface. In addition, the pressure of the fluid results in an external distributed force on the structure normal to the surface. The combined problem is mathematically expressed as

$$\mathbf{S}(\omega)\mathbf{x}(\omega) = \mathbf{y}(\omega), \tag{7}$$

where the linear operator $\mathbf{S}$ is composed of the BE and FE system matrices and the geometric coupling matrices. The unknown vector $\mathbf{x}$ contains the nodal displacements of the FE model as well as the acoustic pressure at the collocation points for the BE model, and can be found by formally inverting $\mathbf{S}$. The vector $\mathbf{y}$ represents the exciting structural forces and contributions from fixed sources in the acoustic domain. ω is the radian frequency. The pressure field radiated from t he propeller due to axial vibration of the propeller is considered in the system matrix $\mathbf{S}$, as it depends on the axial velocity of the propeller hub. The structural force at the propeller hub and the correlated pressure field due to the operation of the propeller are considered in the vector $\mathbf{y}$. The scattering of the propeller pressure field by the hull and the re-excitation of the hull due to the propeller pressure field is taken into account. The influence of the acoustic pressure field due to hull vibration on the propeller forces is, however, neglected. For the models presented in this work, non-matching meshes have been used. This requires a piecewise relaxation of the continuity condition by means of mortar elements [15].

3.2. Radiated sound power

The sound power radiated through a surface Λ is given by [16]

$$\Pi(\omega) = \frac{1}{2}\int_{\Lambda} p(\omega)v^*(\omega)\,\mathrm{d}\Lambda, \tag{8}$$

where p is the acoustic pressure of the fluid and v is the normal velocity of a fluid particle at the surface. As the radiated sound power of the discrete sources in the fluid domain is not implicitly known, a surface enclosing the sources and the structure has to be chosen in order to evaluate the overall radiated sound power. If the surface Λ is spherical and in the far field with respect to the sound sources, then Eq. (8) simplifies to [17]

$$\Pi(\omega) \approx \frac{1}{2\rho c}\int_{\Lambda} p(\omega)p^*(\omega)\,\mathrm{d}\Lambda, \tag{9}$$

where ρ is the density of the fluid and c is the speed of sound. The sound pressure can be expressed as a piecewise interpolation, where the pressure is given at a set of discrete points. For the purpose of integration, Gaussian integration points are chosen to interpolate the pressure. A discrete version of Eq. (9) is obtained, by considering the fluid and geometry properties of the surface Λ in a matrix

$$\Pi(\omega) = \mathbf{p}^{\mathrm{H}}(\omega)\boldsymbol{\Theta}\mathbf{p}(\omega), \tag{10}$$

where the superscript 'H' denotes the conjugate transpose. If $\mathbf{x}$ is known, then the vector of discrete pressures $\mathbf{p}$ on the surface Λ can be explicitly obtained by [18]

$$\mathbf{p}(\omega) = \mathbf{T}(\omega)\mathbf{x}(\omega) + \mathbf{p}_{\mathrm{inc}}(\omega). \tag{11}$$

The transfer matrix $\mathbf{T}$ is obtained by integration over the vibrating surface of the structure and $\mathbf{p}_{\mathrm{inc}}$ represents the pressure contribution from discrete sources in the fluid domain at the integration points of the surface Λ.

3.3. Sensitivity analysis

The sensitivity of the radiated sound power to a set of structural design parameters $\boldsymbol{\vartheta}$ of the vibrating structure, that do not have an influence on the scatterer's surface geometry, is obtained by differentiation of Eq. (10). Omitting the ω dependence, this can be written as

$$\frac{\partial \Pi}{\partial \boldsymbol{\vartheta}} = 2\mathbf{p}^{\mathrm{H}}\boldsymbol{\Theta}\frac{\partial \mathbf{p}}{\partial \boldsymbol{\vartheta}}. \tag{12}$$

The sensitivity of the pressure at the integration points with respect to the design parameters is obtained by differentiation of Eq. (11)

$$\frac{\partial \mathbf{p}}{\partial \boldsymbol{\vartheta}} = \mathbf{T}\frac{\partial \mathbf{x}}{\partial \boldsymbol{\vartheta}}. \tag{13}$$

In order to obtain an expression for the sensitivity of the vector $\mathbf{x}$ with respect to the design parameters, Eq. (7) has to be differentiated which yields

$$\mathbf{S}\frac{\partial \mathbf{x}}{\partial \boldsymbol{\vartheta}} + \frac{\partial \mathbf{S}}{\partial \boldsymbol{\vartheta}}\mathbf{x} = \frac{\partial \mathbf{y}}{\partial \boldsymbol{\vartheta}}. \tag{14}$$

Eq. (14) can then be reordered such that an expression for the sensitivity of the vector $\mathbf{x}$ with respect to the design parameters is obtained and is given by

$$\frac{\partial \mathbf{x}}{\partial \boldsymbol{\vartheta}} = \mathbf{S}^{-1}\left(\frac{\partial \mathbf{y}}{\partial \boldsymbol{\vartheta}} - \frac{\partial \mathbf{S}}{\partial \boldsymbol{\vartheta}}\mathbf{x}\right). \tag{15}$$

In order to compute the sensitivity of the sound power, Eqs. (12)–(14) can be combined in an adjoint operator formulation [4]

$$\frac{\partial \Pi}{\partial \boldsymbol{\vartheta}} = 2\mathbf{p}^{\mathrm{H}}\boldsymbol{\Theta}\mathbf{T}\mathbf{S}^{-1}\left(\frac{\partial \mathbf{y}}{\partial \boldsymbol{\vartheta}} - \frac{\partial \mathbf{S}}{\partial \boldsymbol{\vartheta}}\mathbf{x}\right). \tag{16}$$

Let $\mathbf{b}^{\mathrm{T}} = 2\mathbf{p}^{\mathrm{H}}\boldsymbol{\Theta}\mathbf{T}$ and $\mathbf{z}^{\mathrm{T}} = \mathbf{b}^{\mathrm{T}}\mathbf{S}^{-1}$, then the sensitivity of the sound power can be found for any set of parameters $\boldsymbol{\vartheta}$, as long as the solution of the system of equations $\mathbf{S}^{\mathrm{T}}\mathbf{z} = \mathbf{b}$ is known. This means that for an arbitrary number of structural design parameters, only two systems of equations have to be solved.

3.4. Optimisation

For optimisation of the resonance changer parameters, the following cost function has been defined to represent the radiated sound power over the frequency range of interest [4]

$$J = \frac{1}{\Delta\omega}\int_{\omega} \Pi(\omega)\,\mathrm{d}\omega. \tag{17}$$

The gradient of the cost function can be obtained by differentiating Eq. (17) with respect to the design parameters

$$\frac{\partial J}{\partial \boldsymbol{\vartheta}} = \frac{1}{\Delta\omega}\int_{\omega} \frac{\partial \Pi(\omega)}{\partial \boldsymbol{\vartheta}}\,\mathrm{d}\omega. \tag{18}$$

The problem of minimising the radiated sound power can be written as

$$\text{minimise} \quad J(\boldsymbol{\vartheta}) \text{ subject to } \quad \underline{\boldsymbol{\vartheta}} \le \boldsymbol{\vartheta} \le \overline{\boldsymbol{\vartheta}}, \tag{19}$$

where $\underline{\boldsymbol{\vartheta}}$ and $\overline{\boldsymbol{\vartheta}}$ are the lower and upper bounds for the design parameters, respectively. As the first derivatives of the cost function J with respect to the design parameters $\boldsymbol{\vartheta}$ are explicitly available, an appropriate family of methods to find local minima are the quasi-Newton algorithms [19]. An example of such an algorithm that is applicable to Eq. (19) is the limited memory Broyden–Fletcher–Goldfarb–Shanno algorithm with parameter bounds (L-BFGS-B) [20]. However, applying the L-BFGS-B directly to Eq. (19) can require a large number of computationally expensive cost function evaluations. In addition, the process can get easily trapped in a numerically related local minimum. In order to reduce the number of required evaluations of J and $\partial J/\partial\boldsymbol{\vartheta}$, an iterative algorithm can be applied, where the problem is locally approximated by an explicit subproblem

$$\text{minimise} \quad F(\boldsymbol{\vartheta})^{(k)} \text{ subject to } \quad \underline{\boldsymbol{\vartheta}}^{(k)} \le \boldsymbol{\vartheta} \le \overline{\boldsymbol{\vartheta}}^{(k)} \tag{20}$$

for an iteration point k. The subproblem is solved using the L-BFGS-B. The optimum parameters for the subproblem represent the next iteration point and the formulation for the next subproblem is modified based on data from previous iterations. The iteration is stopped when certain convergence criteria are fulfilled. An example for this approach is the method of moving asymptotes (MMA), where asymptotes are used to approximate the cost function [21]. For the algorithm used in this paper, inner iterations l are conducted in addition to the outer iterations k. This approach is called the globally convergent method of moving asymptotes (GCMMA) [12]. The cost function is approximated near the iteration points using

$$F(\boldsymbol{\vartheta})^{(k,l)} = \sum_{i=1}^{n}\left(\frac{q_i^{(k,l)}}{\vartheta_i^{(k)} - \vartheta_i + \sigma_i^{(k)}} + \frac{r_i^{(k,l)}}{\vartheta_i - \vartheta_i^{(k)} + \sigma_i^{(k)}} - \frac{q_i^{(k,l)} + r_i^{(k,l)}}{\sigma_i^{(k)}}\right) + J(\boldsymbol{\vartheta}^{(k)}), \tag{21}$$

where n represents the number of parameters, i is the index for a parameter, $\boldsymbol{\vartheta}^{(k)}$ represents the optimal solution from the last outer iteration step and $\boldsymbol{\sigma}^{(k)}$ are the moving asymptotes. The asymptotes are moved after each outer iteration. If the process oscillates, the asymptotes are moved closer to the iteration point to make the approximation more conservative. In contrast, if the process is slow, the asymptotes are moved away from the iteration point. The coefficients $q_i^{(k,l)}$ and $r_i^{(k,l)}$ are given by

$$q_i^{(k,l)} = (\sigma_i^{(k)})^2 \max\left\{0, \frac{\partial J_i}{\partial \vartheta_i}(\boldsymbol{\vartheta}^{(k)})\right\} + \frac{\psi^{(k,l)}\sigma_i^{(k)}}{4}, \tag{22}$$

$$r_i^{(k,l)} = (\sigma_i^{(k)})^2 \max\left\{0, -\frac{\partial J_i}{\partial \vartheta_i}(\boldsymbol{\vartheta}^{(k)})\right\} + \frac{\psi^{(k,l)}\sigma_i^{(k)}}{4}, \tag{23}$$

where the parameter $\psi^{(k,l)}$ is adjusted for the inner iteration in order to achieve global convergence. This is accomplished by increasing $\psi^{(k,l)}$ until $J(\hat{\boldsymbol{\vartheta}}^{(k,l)})$ is smaller than $F(\hat{\boldsymbol{\vartheta}}^{(k,l)})$, where $\hat{\boldsymbol{\vartheta}}^{(k,l)}$ denotes the optimal solution for the subproblem of the inner iteration. Subsequently $\hat{\boldsymbol{\vartheta}}^{(k,l)}$ becomes the next outer iteration point $\boldsymbol{\vartheta}^{(k)}$. Rules for updating the parameters $\boldsymbol{\sigma}^{(k)}$ and $\psi^{(k,l)}$ and for the definition of $\underline{\boldsymbol{\vartheta}}^{(k)}$ and $\overline{\boldsymbol{\vartheta}}^{(k)}$ can be found in Ref. [12].

4. Results

Results are presented for the optimisation of the RC virtual damping, stiffness and mass parameters using different cost functions. Results are also given for the sensitivity of some cost functions to these parameters near the optimum. ANSYS 11 was used to generate the FE and BE meshes and to compute the FE stiffness, mass and damping matrices. All other computations were conducted using software implemented in SciPy and C++. For efficient generation of the results, the calculation of the cost function has been parallelised with respect to the frequency using the message passing interface (MPI), by employing a method similar to that described in Ref. [22]. Integration over the frequency range was implemented in an adaptive manner by comparing results for the Simpson rule to results for the trapezium rule. A minimum number of 210 integration points was used. System matrices that are independent of the design parameters have been precomputed and stored in a database at a step size of 0.1 Hz.

Properties of the submarine's propeller/shafting system and hull are given in Tables 1 and 2, respectively. By taking into account physical feasibility as described in Ref. [10], the RC virtual damping was varied between 5×10^3 and 1.1×10^6 kg/s. Ranges from 1.5×10^7 to 1.5×10^9 N/m and from 1 to 20 tonnes were chosen for the RC virtual stiffness and mass, respectively.

Table 1
Properties of the propeller/shafting system.

Parameter	Value	Unit
Propeller diameter	3.25	m
Propeller structural mass	10	tonnes
Propeller added mass of water	11.443	tonnes
Shaft Young's modulus	200	GPa
Shaft Poisson's ratio	0.3	
Shaft density	7800	kg/m^3
Shaft cross-sect. area	0.071	m^2
Shaft length	10.5	m
Effective shaft length	9	m
Bearing mass	0.2	tonnes
Bearing stiffness	2×10^{10}	N/m
Bearing damping	3×10^5	kg/s
Resonance changer mass	1	tonne
Foundation major radius	1.25	m
Foundation minor radius	0.52	m
Foundation half angle	15	deg
Foundation thickness	10	mm
Foundation Young's modulus	200	GPa
Foundation density	7800	kg/m^3

Table 2
Properties of the hull.

Parameter	Value	Unit
Cylinder length	45.0	m
Cylinder radius	3.25	m
Shell thickness	0.04	m
Stiffener cross-sectional area	0.012	m^2
Stiffener spacing	0.5	m
Young's modulus of structure without foundation	210	GPa
Young's modulus of foundation	200	GPa
Poisson ratio of structure	0.3	
Density of structure	7800	kg/m^3
Structural loss factor	0.02	
Added mass	796	kg/m^2
Stern lumped mass	188	tonnes
Bow lumped mass	200	tonnes
Cone half angle	24	deg
Cone length	9.079	m
Cone smaller radius	0.3	m
Density of fluid	1000	kg/m^3
Speed of sound	1500	m/s

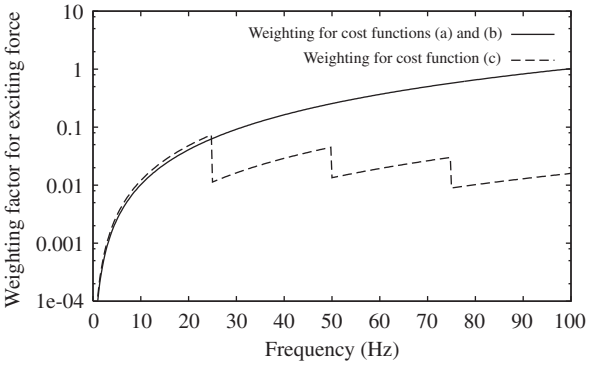

Fig. 3. Weighting functions for the force used in the three cost functions.

4.1. Optimisation

The optimisation was conducted using the GCMMA for different cost functions, where eight different initial parameter sets were used. The initial parameter sets were obtained by dividing each dimension of the three-dimensional parameter space by three, where the intersections of the dividing borders form the initial parameter sets. The iterations were stopped when the cost function values differed by less than 1^{-20} W between two subsequent iterations. An optimisation run for a single initial parameter set required an average of 40 min on a computer cluster of six 3 GHz Pentium 4 CPUs. Each of the processors has 2 Gb RAM. The cluster nodes were connected using a gigabit ethernet. Three different cost functions have been investigated. For cost function (a), sound radiation due to propeller vibration was neglected. This means that re-excitation of the hull due to the propeller pressure field caused by propeller vibration was not taken into account. The sound power radiated from the submarine was only due to the pressure field from the hull and the propeller pressure field due to the operation of the propeller in a non-uniform wake. A single axial exciting force at the propeller hub that ranges from 1 to 100 Hz was considered. The force was weighted with $(\omega/\Delta\omega)^2$, as it increases proportionally with the square of the radian frequency. For cost function (b), the exciting force was weighted as for cost function (a), but sound radiation due to propeller vibration has been taken into account. This means that the hull experiences re-excitation due to the additional propeller pressure field. The contribution of the propeller pressure field due to propeller vibration to the overall radiated sound power is also considered. For cost function (c), sound radiation due to propeller vibration was taken into account. Furthermore it has been assumed that the exciting force is a superposition of the first four harmonics of *bpf* and that the relative force amplitude is smaller for higher harmonics of *bpf*. Under the assumption that the propeller diameter is half the hull diameter and the tip speed is limited to 40 m/s to avoid cavitation, for a 7-bladed propeller the maximum fundamental *bpf* is approximately 25 Hz. The force amplitude for higher harmonics of *bpf* was assumed to be $1/n$ times the force amplitude for *bpf* at a given shaft speed for the n th harmonic of *bpf*. The cost function is computed by superposition of the contributions from the individual harmonics of *bpf*. The superposition can be considered implicitly during integration over the frequency range. The resulting weighting factors for the exciting force are shown in Fig. 3 for the three cost functions.

The optimisation results are given in Tables 3–5 for cost functions (a), (b) and (c), respectively. For cost function (a), six out of the eight sets of initial parameters lead to a common minimum with a function value of around 7.19×10^{-13} W (for three digits of accuracy). The optimum RC parameters for the lowest function value of 7.1865×10^{-13} W are given by $c_r = 4.3657 \times 10^5$ kg/s, $k_r = 3.0024 \times 10^8$ N/m and $m_r = 1$ tonne. For cost function (b), seven out of the eight sets of initial parameters lead to a common minimum with a function value of around 2.6745×10^{13} W. The optimum parameters are given by $c_r = 1.1 \times 10^6$ kg/s, $k_r = 5.3818 \times 10^8$ N/m and $m_r = 1$ tonne. For cost function (c), all eight sets of initial parameters lead to a common minimum with a function value of around 8.3337×10^{-14} W. The optimum parameters for this function value are given by $c_r = 5 \times 10^3$ kg/s, $k_r = 1.5 \times 10^7$ N/m and $m_r = 1$ tonne. It should be noted that all of the cost functions result in the lower limit of 1 tonne for the optimum RC virtual mass.

In order to compare the performance of the optimum RC parameters from the three cost functions, the radiated sound power for the submarine model with and without the use of an RC are compared in Fig. 4, where structural excitation from the propeller, dipole excitation due to the operation of the propeller in a non-uniform wake and dipole excitation due to propeller vibration have been considered. The exciting force was weighted by $(\omega/\Delta\omega)^2$. The peaks in the radiated sound power at around 20, 45 and 70 Hz represent the first three axial hull resonances. The maximum sound radiation occurs at the fundamental propeller/shafting system resonance which occurs at 37.3 Hz. Results were also obtained for the sound power level using RC parameters according to Goodwin [8], in which the natural frequency of the RC is tuned to match the natural frequency of the propeller/shafting system. The RC virtual mass was chosen to be at the lower parameter bound of $m_r = 1$ tonne, as proposed by Goodwin. In addition, the lower limit of $m_r = 1$ tonne for the RC virtual mass was obtained

Table 3
Optimisation results for cost function (a).

Parameters c_r (kg/s) k_r (N/m) m_r (tonnes) Initial	Optimum	Function value J (W)	Outer iterations
3.70×10^5 5.10×10^8 7.33×10^3	5.48×10^5 7.29×10^8 2.87×10^3	7.68×10^{-13}	32
7.35×10^5 5.10×10^8 7.33×10^3	4.30×10^5 2.95×10^8 1.00×10^3	7.19×10^{-13}	10
3.70×10^5 1.00×10^9 7.33×10^3	4.39×10^5 2.98×10^8 1.00×10^3	7.19×10^{-13}	12
7.35×10^5 1.00×10^9 7.33×10^3	4.37×10^5 3.00×10^8 1.00×10^3	7.19×10^{-13}	12
3.70×10^5 5.10×10^8 1.37×10^4	4.54×10^5 2.79×10^8 1.00×10^3	7.19×10^{-13}	16
7.35×10^5 5.10×10^8 1.37×10^4	1.10×10^6 7.90×10^8 2.00×10^4	1.54×10^{-12}	6
3.70×10^5 1.00×10^9 1.37×10^4	4.50×10^5 2.75×10^8 1.00×10^3	7.19×10^{-13}	13
7.35×10^5 1.00×10^9 1.37×10^4	4.42×10^5 2.80×10^8 1.00×10^3	7.19×10^{-13}	14

during the optimisation process, as well as in Ref. [9]. The RC virtual stiffness is obtained using [8]

$$k_r = 4\pi^2 f_{ps}^2 m_r, \tag{24}$$

where $f_{ps} = 37.3$ Hz is the fundamental resonance frequency of the propeller/shafting system. This yields an RC virtual stiffness of $k_r = 5.48 \times 10^{10}$ N/m. The RC virtual damping parameter is calculated using [8]

$$c_r = \sqrt{\frac{m_r k_r q}{4}\left(6 + q + \sqrt{8q + q^2}\right)}, \tag{25}$$

where $q = 4\pi^2 f_{ps}^2 m_p / k_r$. This yields an RC virtual damping of $c_r = 3.93 \times 10^6$ kg/s. Using Goodwin's method, a reduction of the sound power level can be observed for frequencies between 10 and 75 Hz. For the majority of the frequency range, the radiated sound power for a submarine model with no RC is significantly higher than for submarine model with an RC that has been optimised using any of the cost functions. The curves for cost functions (a) and (b) are similar, but the radiated sound power for cost function (b) is slightly lower for frequencies above about 70 Hz. This is attributed to the fact that the sound radiation in the high frequency range is strongly correlated to propeller vibration which is accounted for in cost function (b). A higher RC virtual damping obtained using cost function (b) therefore leads to a decrease of radiated sound power at higher frequencies. For cost function (c), the sound radiation has been significantly decreased in the low frequency range and slightly increased in the high frequency range. This means that sound radiation from the propeller does not have a significant influence on the optimisation using cost function (c) due to the assumption that the amplitude for higher harmonics of *bpf* is only a fraction of the amplitude for the fundamental *bpf*. This leads to a very resilient propeller/shafting system due to the small RC virtual stiffness.

4.2. Sensitivity analysis

The sensitivity of the cost functions (b) and (c) to the RC virtual damping and stiffness is investigated, in order to assess the influence of RC parameters on the radiated sound power. The sensitivity of the cost functions to the RC virtual mass has been omitted as all investigated cost functions lead to the same RC virtual mass of 1 tonne. This value has also been found

Table 4
Optimisation results for cost function (b).

Parameters c_r (kg/s) k_r (N/m) m_r (tonnes) Initial	Optimum	Function value J (W)	Outer iterations
3.70×10^5 5.10×10^8 7.33×10^3	1.10×10^6 5.44×10^8 1.00×10^3	2.67×10^{-13}	9
7.35×10^5 5.10×10^8 7.33×10^3	1.10×10^6 5.35×10^8 1.00×10^3	2.67×10^{-13}	8
3.70×10^5 1.00×10^9 7.33×10^3	1.10×10^6 5.44×10^8 1.00×10^3	2.67×10^{-13}	8
7.35×10^5 1.00×10^9 7.33×10^3	1.10×10^6 5.36×10^8 1.00×10^3	2.67×10^{-13}	8
3.70×10^5 5.10×10^8 1.37×10^4	1.10×10^6 5.38×10^8 1.00×10^3	2.67×10^{-13}	11
7.35×10^5 5.10×10^8 1.37×10^4	1.10×10^6 1.14×10^9 2.00×10^4	9.18×10^{-13}	19
3.70×10^5 1.00×10^9 1.37×10^4	1.10×10^6 5.47×10^8 1.00×10^3	2.67×10^{-13}	9
7.35×10^5 1.00×10^9 1.37×10^4	1.10×10^6 5.46×10^8 1.00×10^3	2.67×10^{-13}	8

previously by Dylejko [10]. A sensitivity analysis for cost function (a) has not been considered as cost functions (b) and (c) are assumed to be more relevant as they include the sound radiation due to propeller vibration. For the sensitivity analyses presented here, the optimum RC virtual mass parameter of 1 tonne has been used.

Results for cost function (b) are given in Fig. 5, where an increase of the RC virtual damping leads to lower values for J. Two distinct local maxima of the cost function can be identified. The first local maximum occurs at the upper limit for k_r and the lower limit for c_r. The second local maximum occurs at the lower limit for both the RC virtual stiffness k_r and damping c_r. The variation of sound power with frequency is shown in Fig. 6 for the corresponding RC parameters. For the first local maximum, the cost function is dominated by sound radiation at the fundamental propeller/shafting system resonance. In this case, the fundamental resonance of the propeller/shafting system has been decreased by 10–27 Hz when compared to the configuration with no RC. For the second local maximum, the cost function is dominated by the sound power due to propeller vibration in the high frequency range as a decrease of the values for c_r and k_r involves an increase of the propeller/shafting system axial flexibility. For the minimum cost function value, the fundamental hull resonance occurs at around 15 Hz. Due to the frequency weighting, the contribution of the radiated sound power to the cost function is small at this frequency.

The sensitivity of the cost function with respect to the virtual damping and the virtual stiffness of the resonance changer is shown in Figs. 7 and 8, respectively. The plots indicate that the first maximum of the cost function at the lower limits of the RC parameters is primarily sensitive to the RC stiffness, whereas the second maximum of the cost function at the lower limit of the RC virtual damping and the upper limit of the RC virtual stiffness is primarily sensitive to the RC virtual damping. It can be concluded that an increase in RC virtual stiffness reduces axial propeller vibration in the higher frequency range. An increase in RC virtual damping will primarily lower sound radiation at the propeller/shafting system fundamental resonance.

Cost function (c), where the decrease in amplitude for higher harmonics of bpf was considered, is shown in Fig. 9. The values for J are much lower than in Fig. 5, as the influence of sound radiation at higher frequencies on the cost function has been reduced. There is only one global maximum due to the propeller/shafting system resonance. Direct sound radiation from the propeller in the high frequency range does not have a significant impact. As k_r increases, the propeller/shafting system fundamental resonance increases and the overall sound radiation becomes larger as the exciting force is weighted

Table 5
Optimisation results for cost function (c).

Parameters c_r (kg/s) k_r (N/m) m_r (tonnes) Initial	Optimum	Function value J (W)	Outer iterations
3.70×10^5 5.10×10^8 7.33×103	5.00×10^3 1.50×10^7 1.00×10^3	8.33×10^{-14}	9
7.35×10^5 5.10×10^8 7.33×103	5.00×10^3 1.50×10^7 1.00×10^3	8.33×10^{-14}	10
3.70×10^5 1.00×10^9 7.33×103	5.00×10^3 1.50×10^7 1.00×10^3	8.33×10^{-14}	10
7.35×10^5 1.00×10^9 7.33×103	5.00×10^3 1.50×10^7 1.00×10^3	8.33×10^{-14}	10
3.70×10^5 5.10×10^8 1.37×104	5.00×10^3 1.50×10^7 1.00×10^3	8.33×10^{-14}	16
7.35×10^5 5.10×10^8 1.37×104	5.00×10^3 1.50×10^7 1.00×10^3	8.33×10^{-14}	12
3.70×10^5 1.00×10^9 1.37×104	5.00×10^3 1.50×10^7 1.00×10^3	8.33×10^{-14}	12
7.35×10^5 1.00×10^9 1.37×104	5.00×10^3 1.50×10^7 1.00×10^3	8.33×10^{-14}	13

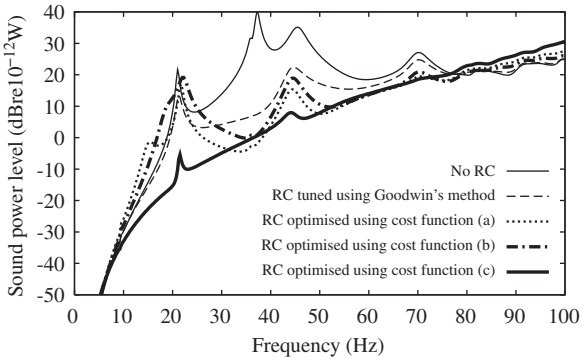

Fig. 4. Sound power level with no RC, with an RC tuned using Goodwin's method [8] and using the optimum RC parameters for the three cost functions.

with the square of the frequency. However, as the propeller/shafting system fundamental resonance becomes higher than the upper frequency limit for the first harmonic of *bpf*, the value for J drops. This can be predicted from the weighting function applied to the exciting force for cost function (c) shown in Fig. 3. The radiated sound power over the investigated frequency range for the weighted exciting force is shown in Fig. 10. For the maximum value of J, the fundamental resonance of the propeller/shafting system can be identified near 25 Hz. At the curve for the minimum value of J, the fundamental resonance of the propeller/shafting system cannot be identified and the maximum sound radiation is due to the first axial hull resonance. The sound radiation in the high frequency range is slightly higher for the RC configuration that corresponds to a minimum for J. However, this does not have a significant influence on J, as J is dominated by contributions that can be attributed to the first harmonic of *bpf*.

The sensitivity of the cost function to the RC virtual damping and stiffness is shown in Figs. 11 and 12, where a *bpf* weighted exciting force has been used. Both, the RC virtual stiffness and damping have considerable influence on the cost function at the global maximum. However, for a large part of the parameter space, the cost function is relatively stable. This

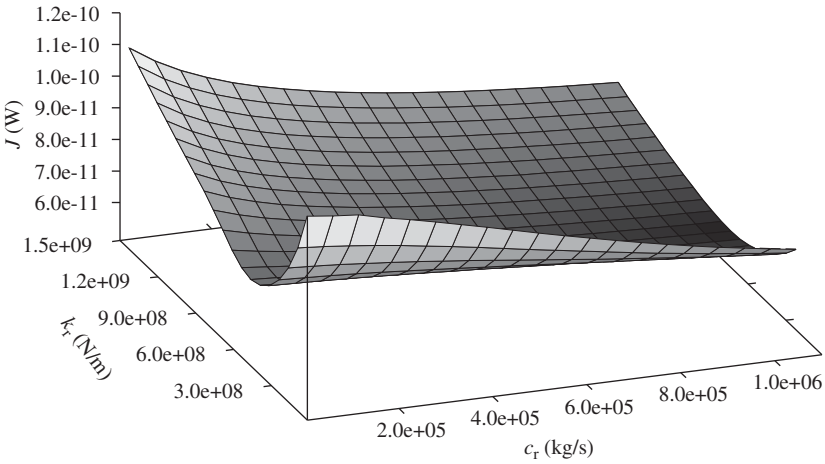

Fig. 5. Cost function (b).

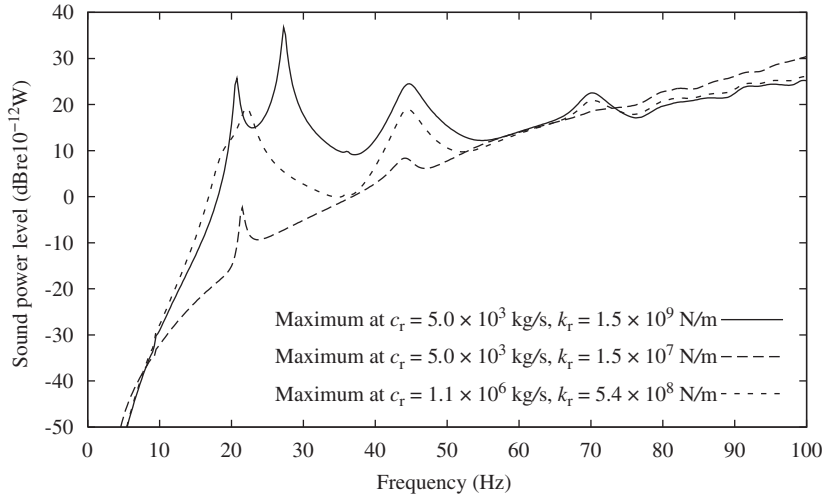

Fig. 6. Radiated sound power for the minimum and maximum values of cost function (b).

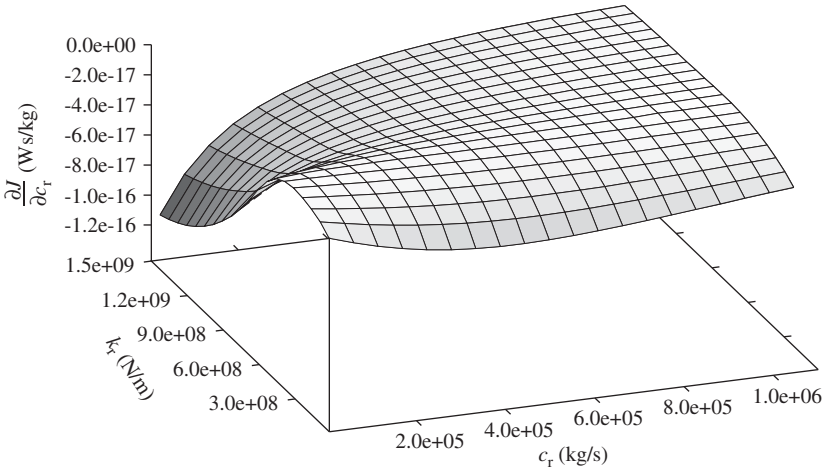

Fig. 7. Sensitivity of cost function (b) with respect to RC damping.

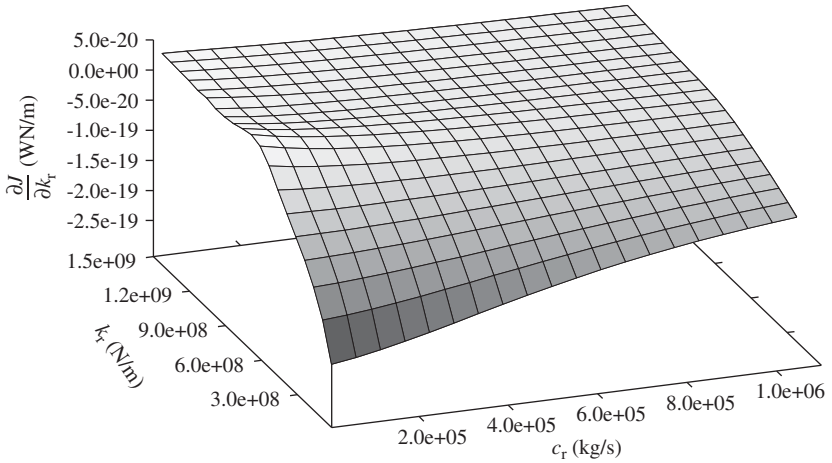

Fig. 8. Sensitivity of cost function (b) with respect to RC stiffness.

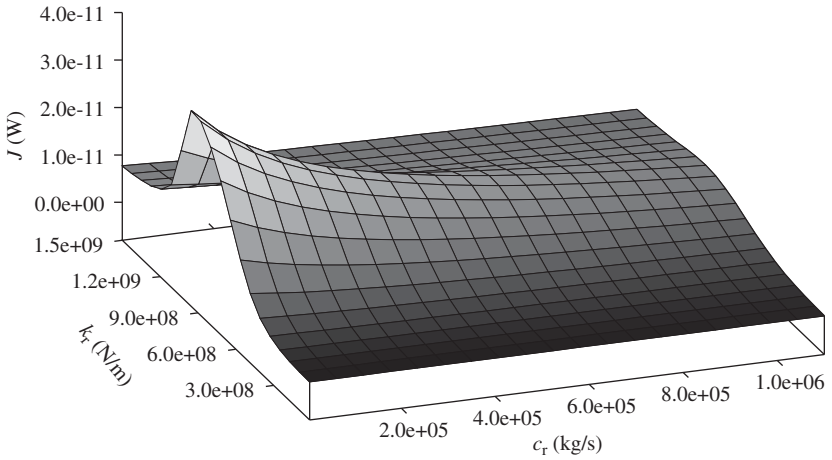

Fig. 9. Cost function (c).

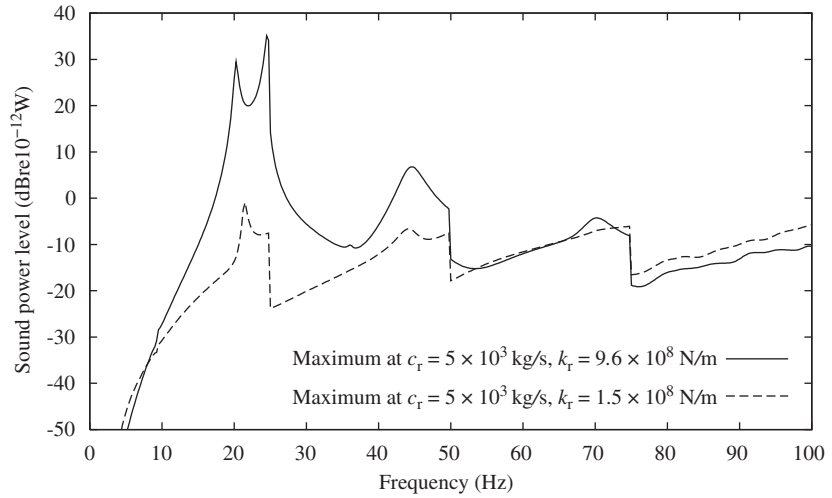

Fig. 10. Radiated sound power for the minimum and maximum values of cost function (c).

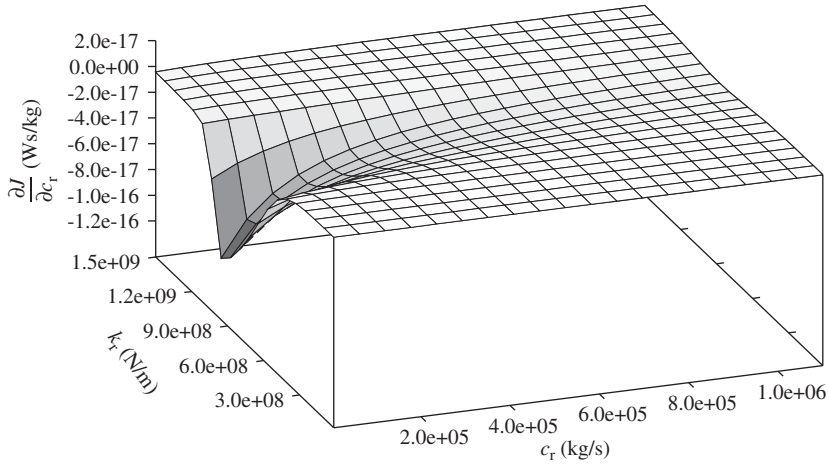

Fig. 11. Sensitivity of cost function (c) with respect to RC damping.

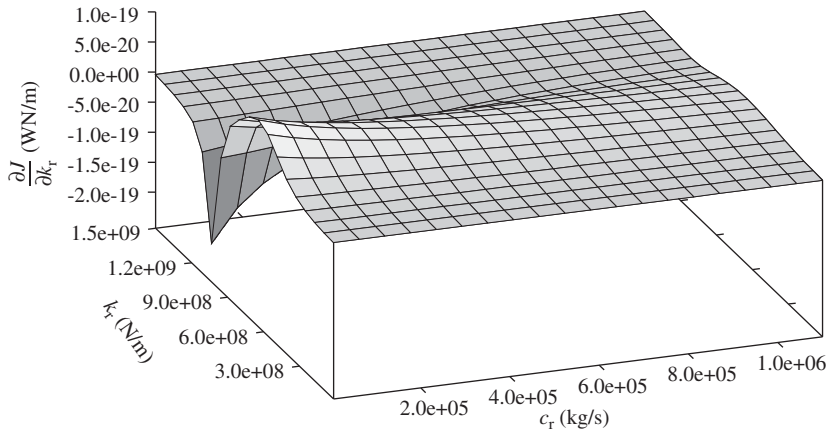

Fig. 12. Sensitivity of cost function (c) with respect to RC stiffness.

means that a wide variety of RC parameter configurations is available to provide efficient reduction of the overall radiated sound power.

5. Conclusions

A fully coupled vibro-acoustic model for a submarine has been developed in order to find optimum design parameters for a passive vibration attenuation device known as a resonance changer. The objective is to minimise the overall radiated sound power due to propeller forces in the low frequency range. The overall radiated sound power is due to both sound radiated from the hull as well as sound radiated from the propeller. Cost functions have been obtained by integration of the frequency-weighted radiated sound power over the frequency range of interest. In order to use gradient based optimisation, the sensitivity of the cost function to the design parameters was also computed using an adjoint operator formulation. The globally convergent method of moving asymptotes has been applied in conjunction with the L-BFGS-B method to find the optimum virtual damping, stiffness and mass parameters for the resonance changer. With respect to the parameter space, eight equally distributed initial parameter sets have been used, where at least six optimisation runs resulted in a common minimum.

The influence of sound radiation due to propeller vibration as well as the influence of the reduction in amplitude for higher harmonics of the blade-passing frequency on the optimisation has been investigated. It has been shown that inclusion of sound radiation due to propeller vibration leads to a higher RC virtual damping parameter which reduces axial vibration of the propeller/shafting system, and therefore sound radiation due to propeller vibration. When the reduction in amplitude for higher harmonics of *bpf* is considered, the sound radiation due to propeller vibration becomes insignificant which leads to a very resilient configuration of the RC with a low RC virtual stiffness and damping.

For the more realistic cost functions which consider sound radiation due to propeller vibration, the parameter space has been visualised by keeping one optimum parameter constant. The minimum and the maxima have been analysed. For the global minimum, the fundamental resonance of the propeller/shafting system occurs below the fundamental hull resonance and does not have a significant influence on the cost function value due to the frequency weighting.

References

[1] J.S. Carlton, *Marine Propellers and Propulsion*, Butterworth-Heinemann, Oxford, 1994.
[2] O. Rath Spivack, R. Kinns, N. Peake, Acoustic excitation of hull surfaces by propeller sources, *Journal of Marine Science Technology* 9 (2004) 109–116.
[3] C. Norwood, The free vibration behaviour of ring stiffened cylinders, Technical Report 200, DSTO Aeronautical and Maritime Research Laboratory, Melbourne, Australia, 1995.
[4] S. Marburg, Developments in structural–acoustic optimization for passive noise control, *Archives of Computational Methods in Engineering* 9 (4) (2002) 291–370.
[5] O.C. Zienkiewicz, R.L. Taylor, *The Finite Element Method*: *Solid Mechanics*, Vol. 2, sixth ed., Elsevier, Butterworth-Heinemann, Amsterdam, London, 2005.
[6] C.A. Brebbia, R.D. Ciskowski, *Boundary Element Methods in Acoustics*, Elsevier Applied Science, New York, 1991.
[7] S. Amini, P.J. Harris, D.T. Wilton, *Coupled Boundary and Finite Element Methods for the Solution of the Dynamic Fluid–Structure Interaction Problem*, Springer, Berlin, New York, 1992.
[8] A.J.H. Goodwin, The design of a resonance changer to overcome excessive axial vibration of propeller shafting, *Transactions of the Institute of Marine Engineers* 72 (1960) 37–63.
[9] P.G. Dylejko, N.J. Kessissoglou, Y.K. Tso, C.J. Norwood, Optimisation of a resonance changer to minimise the vibration transmission in marine vessels, *Journal of Sound and Vibration* 300 (2007) 101–116.
[10] P.G. Dylejko, Optimum Resonance Changer for Submerged Vessel Signature Reduction, PhD Thesis, The University of New South Wales, Sydney, Australia, 2008.
[11] S. Merz, R. Kinns, N.J. Kessissoglou, Structural and acoustic responses of a submarine hull due to propeller forces, *Journal of Sound and Vibration* 325 (2009) 266–286.
[12] K. Svanberg, A class of globally convergent optimization methods based on conservative convex separable approximations, *SIAM Journal on Optimization* 12 (2) (2002) 555–573.
[13] P.M. Morse, K.U. Ingard, *Theoretical Acoustics*, McGraw-Hill, New York, 1968.
[14] T. Mellow, L. Kärkkäinen, On the sound field of an oscillating disk in a finite open and closed circular baffle, *Journal of the Acoustical Society of America* 118 (3) (2005) 1311–1325.
[15] F.B. Belgacem, The mortar finite element method with Lagrange multipliers, *Numerische Mathematik* 84 (2) (1999) 173–197.
[16] T.W. Wu (Ed.), *Boundary Element Acoustics*, WIT Press, Southampton, UK, 2000.
[17] D. Ross, *Mechanics of Underwater Noise*, Penninsula Publishing, Los Altos, CA, 1987.
[18] S. Merz, N.J. Kessissoglou, R. Kinns, Influence of resonance changer parameters on the radiated sound power of a submarine, *Acoustics Australia* 37 (2009) 12–17.
[19] R.T. Haftka, Z. Gurdal, *Elements of Structural Optimization*, third ed., Kluwer Academic Publishers, Boston, MA, 1992.
[20] R.H. Byrd, P. Lu, J. Nocedal, C. Zhu, A limited memory algorithm for bound constrained optimization, *SIAM Journal on Scientific Computing* 16 (5) (1995) 1190–1208.
[21] K. Svanberg, The method of moving asymptotes—a new method for structural optimization, *International Journal for Numerical Methods in Engineering* 24 (2) (1987) 359–373.
[22] V.A. Miller, G.J. Davis, Adaptive quadrature on a message-passing multiprocessor, *Journal of Parallel and Distributed Computing* 14 (4) (1992) 417–425.